NASA TECHNICAL MEMORANDUM

NASA TM X-71903

NASA TM X-71903

A THEORETICAL STUDY OF THE ACOUSTIC IMPEDANCE OF ORIFICES IN THE PRESENCE OF A STEADY GRAZING FLOW

by Edward J. Rice
Lewis Research Center
Cleveland, Ohio 44135

TECHNICAL PAPER to be presented at
Ninety-first Meeting of the Acoustical
Society of America
Washington, D. C., April 5-9, 1976

A THEORETICAL STUDY OF THE ACOUSTIC IMPEDANCE OF ORIFICES IN THE PRESENCE OF A STEADY GRAZING FLOW

by Edward J. Rice

E-8692

ABSTRACT

An analysis of the oscillatory fluid flow in the vicinity of a circular orifice with a steady grazing flow is presented. The study is similar to that of Hersh and Rogers but with the addition of the grazing flow. Starting from the momentum and continuity equations, a considerably simplified system of partial differential equations is developed with the assumption that the flow can be described by an oscillatory motion superimposed upon the known steady flow. The equations are seen to be linear in the region where the grazing flow effects are dominant, and a solution and the resulting orifice impedance are presented for this region. The nonlinearity appears to be unimportant for the usual conditions found in aircraft noise suppressors. Some preliminary conclusions of the study are that orifice resistance is directly proportional to grazing flow velocity (known previously from experimental data) and that the orifice inductive (mass reactance) end correction is not a function of grazing flow. This latter conclusion is contrary to the widely held notion that grazing flow removes the effect of the orifice inductive end correction. This conclusion also implies that the experimentally observed total inductance reduction with grazing flow might be in the flow within the orifice rather than in the end correction.

INTRODUCTION

The acoustic impedance of perforated materials in the presence of a steady grazing flow is an essential component of noise suppressor research. This impedance is used as a boundary condition in all duct sound propagation studies.

Several investigations of the grazing flow impedance phenomenon have been performed (Refs. 1 to 11) that lead to impedance models being generated for use in impedance calculations. Theoretical studies of a basic nature have

been performed (Refs. 12 and 13) but mainly without grazing flow. Recent work has been performed which is exposing the basic physics involved in the resistive component of the grazing flow impedance (Refs. 8 and 14), however, the physics of the imaginary or reactive component are yet unclear.

A valuable study has been performed (Ref. 15) which considered the acoustic impedance, both linear and nonlinear, of an orifice without grazing flow. This study is of particular interest since it was derived directly from the Navier-Stokes equations and was thus very basic in nature. Closed form solutions (exact for the linear and approximate for the nonlinear) were obtained for both the real and imaginary component of the acoustic impedance.

The work reported in this paper represents an extension of Reference 15 in that the steady grazing flow is added. A spherically symmetrical flow perturbation is assumed to be impressed upon the known unsymmetrical steady flow. Where the grazing flow effects dominate, the equations are found to be linear thus yielding closed form solutions (with suitable simplifying assumptions) for acoustic pressure and velocity. The expression for acoustic impedance is also presented and the resistive part is compared to acoustic resistance models derived from experiments. The steady orifice flow solutions are also obtained and calculated pressures in the vicinity of the orifice are compared with measured pressures.

SYMBOLS

A_{NL} area dominated by nonlinearity, m^2

A_{TOT} total flow area, m^2

c speed of sound, m/sec

d orifice diameter, m

F(t) function of time (see Eq. (30))

f(t) function of time (see Eq (32))

i $\sqrt{-1}$

M_∞ grazing flow Mach number

M_0	orifice Mach number
$\mathscr{P}$	exciting pressure amplitude far from orifice, N/m^2
p	nondimensional perturbation pressure, $p'/\mathscr{P}$
p^*	complete dimensional pressure (see Eq. (5)), N/m^2
$\bar{p}$	average or ambient pressure, N/m^2
p'	perturbation in pressure, N/m^2
p_s	nondimensional static perturbation pressure
p_s^*	dimension form of p_s, N/m^2
p_∞^*	same as $\mathscr{P}$ except for steady orifice flow, N/m^2
q_∞	dynamic pressure ($\frac{1}{2}\ \bar{\rho}\ V_\infty^2$), N/m^2
r	nondimensional radius (r^*/d)
r^*	dimensional radius, m
r_0	r at orifice radius ($r_0 = \frac{1}{2}$)
t	nondimensional time (ωt^*)
t^*	time, sec
U_0	magnitude of radial perturbation velocity near orifice, m/sec
u	nondimensional radial perturbation velocity (u'/U_0)
u^*	complete dimensional radial velocity (see Eq. (6)), m/sec
$\bar{u}$	radial component of grazing flow velocity (see Eq. (1)), m/sec
u'	radial component of perturbation velocity, m/sec
u_s	same as u but for steady orifice flow
u'_{orf}	orifice perturbation velocity based on flow rate and orifice area, m/sec
u'_{vc}	orifice perturbation velocity at vena-contracta, m/sec
V_∞	grazing flow velocity, m/sec
$\bar{v}$	θ component of grazing flow velocity, m/sec

v^*	complete dimensional θ-component of velocity (see Eq. (7)), m/sec
v'	θ-component of perturbation velocity, m/sec
$\overline{w}$	φ-component of grazing flow velocity, m/sec
w^*	complete dimensional φ-component of velocity (see Eq. (8)), m/sec
w'	φ-component of perturbation velocity, m/sec
δ	phase angle between pressure and velocity
ζ	dimensionless acoustic impedance
θ	polar angular coordinate (see Fig. 1)
λ	wavelength, m
ρ^*	density, kg/m^3
$\overline{\rho}$	average uniform density, kg/m^3
ρ'	density perturbation, kg/m^3
φ	azimuthal angular coordinate (see Fig. 1)
ω	circular frequency, rad/sec

THEORETICAL DEVELOPMENT

In this section first the differential equations will be presented in dimensionless form. Next, they will be simplified by a magnitude analysis and finally the solutions will be derived.

Differential Equations

The geometry of the system considered here is shown in Figure 1. Both rectangular and spherical coordinate systems are shown centered at the orifice center. The steady flow velocity is shown parallel to the x axis and although uniform in the rectangular coordinates, in spherical coordinates the expressions are:

$$\bar{u} = -V_\infty \sin\theta \cos\varphi \tag{1}$$

$$\bar{u} = -V_\infty \cos\theta \cos\varphi \tag{2}$$

$$\bar{w} = V_\infty \sin\varphi \tag{3}$$

The differential equations, for the purpose of brevity, will be given with all of the assumptions inserted. The variables will be considered to be given by the sum of a steady component and a time varying component as,

$$\rho^* = \bar{\rho} + \rho' \tag{4}$$

$$p^* = \bar{p} + p' \tag{5}$$

$$u^* = \bar{u} + u' \tag{6}$$

$$v^* = \bar{v} + v' \tag{7}$$

$$w^* = \bar{w} + w' \tag{8}$$

Asterisks are used here to denote complete dimensional quantities for the dependent variables and dimensional quantities for the coordinates. The isentropic relationship is assumed valid so that

$$p' = c^2\rho' \tag{9}$$

The radial coordinate and time will be nondimensionalized as follows,

$$r^* = rd \tag{10}$$

$$t^* = \frac{t}{\omega} \tag{11}$$

The time varying pressure is normalized by the peak far-field pressure

$$p' = \mathcal{P}p \tag{12}$$

and thus using Equation (9)

$$\rho' = \frac{\mathscr{P}}{c^2} p \tag{13}$$

The time varying radial velocity is normalized by the amplitude near the orifice (U_0) thus

$$u' = U_0 u \tag{14}$$

The perturbation velocity (u'), the complete velocity (u*), and two components of the steady grazing flow ($\bar{u}, \bar{v}$) are shown in the two-dimensional sketch of Figure 2. The simplest possible solution will be sought for the velocity and then tested to see if it has provided any information or insight into the physics of the grazing flow impedance. With this in mind, only axisymmetric perturbations of the velocity will be considered and thus,

$$v' = w' = 0 \tag{15}$$

It should be noted later in the development of the equations that even though the velocity perturbation is axisymmetric, the pressure distribution around the orifice is asymmetric The viscous terms in the momentum equations will not be considered.

With the above assumptions, the equations of motion can be written as follows:

Co. tinuity

$$\left(\frac{\mathscr{P}}{\bar{\rho}c^2}\right)\left(\frac{\omega d}{c}\right)\frac{\partial p}{\partial t} + \left(\frac{U_0}{c}\right)\left(1 + \frac{\mathscr{P}}{\bar{\rho}c^2} p\right)\frac{1}{r^2}\frac{\partial}{\partial r}(r^2 u)$$

$$+ \left(\frac{\mathscr{P}}{\bar{\rho}c^2}\right)\left[\left(\frac{U_0}{c} u + \frac{\bar{u}}{c}\right)\frac{\partial p}{\partial r} + \frac{\bar{v}}{c}\frac{1}{r}\frac{\partial p}{\partial \theta} + \frac{\bar{w}}{c}\frac{1}{r \sin\theta}\frac{\partial p}{\partial \varphi}\right] = 0 \tag{16}$$

r-Momentum

$$\left(\frac{\omega d}{c}\right)\frac{\partial u}{\partial t} + \left(\frac{\bar{u}}{c} + \frac{U_0}{c}u\right)\frac{\partial u}{\partial r} + \left(\frac{\mathscr{P}}{\bar{\rho}cU_0}\right)\frac{1}{\left(1 + \frac{\mathscr{P}}{\bar{\rho}c^2}p\right)}\frac{\partial p}{\partial r} = 0 \tag{17}$$

θ-Momentum

$$\left(\frac{\mathscr{P}}{\bar{\rho}cU_0}\right)\frac{1}{\left(1 + \frac{\mathscr{P}}{\bar{\rho}c^2}p\right)}\frac{\partial p}{\partial \theta} + \frac{\bar{v}}{c}u = 0 \tag{18}$$

φ-Momentum

$$\left(\frac{\mathscr{P}}{\bar{\rho}cU_0}\right)\frac{1}{\left(1 + \frac{\mathscr{P}}{\bar{\rho}c^2}p\right)\sin\theta}\frac{\partial p}{\partial \varphi} + \frac{\bar{w}}{c}u = 0 \tag{19}$$

Although considerably simplified from the complete equations, Equations (16) to (19) are still much too complex for a simple closed form solution. An order of magnitude analysis on the coefficients must now be made in a manner similar to Reference 15 except that V_∞ must be considered. Only the coefficients need to be considered since the variables themselves are of order unity due to the nondimensionalization. From several references (Refs. 4, 6, 7, 8, 10, and 14 e.g.) the grazing flow resistance can be approximated by

$$\frac{\mathscr{P}}{\bar{\rho}cU_0} \approx \frac{V_\infty}{c} \tag{20}$$

Thus

$$\frac{\mathscr{P}}{\bar{\rho}c^2} \approx \left(\frac{V_\infty}{c}\right)\left(\frac{U_0}{c}\right) = M_\infty M_0 << 1 \tag{21}$$

since M_∞ is at most 0.6 or 0.7 for the usual acoustic liner and M_0 is much less than this. Also

$$\frac{\omega d}{c} = \frac{2\pi d}{\lambda} << 1 \tag{22}$$

provided the wavelength (λ) is much larger than the orifice diameter (d) which is almost always the case in a practical acoustic liner. The first term in the continuity Equation (16) is probably the smallest of all with the third term being next smallest in magnitude (essentially Mach numbers to the third power when the terms in the square brackets are considered). Also since p is of order unity the term $\mathscr{P}p/\bar{\rho}c^2$ can be dropped where it is added to unity. Thus the problem to be solved is shown to be incompressible and the equations have been reduced to,

$$\frac{\partial}{\partial r}(r^2 u) = 0 \tag{23}$$

$$\left(\frac{\omega d}{c}\right)\frac{\partial u}{\partial t} + \left(\frac{\bar{u}}{c} + \frac{U_0}{c}u\right)\frac{\partial u}{\partial r} + \left(\frac{\mathscr{P}}{\bar{\rho}cU_0}\right)\frac{\partial p}{\partial r} = 0 \tag{24}$$

$$\left(\frac{\mathscr{P}}{\bar{\rho}cU_0}\right)\frac{\partial p}{\partial \theta} + \frac{\bar{v}}{c}u = 0 \tag{25}$$

$$\left(\frac{\mathscr{P}}{\bar{\rho}cU_0}\right)\frac{1}{\sin\theta}\frac{\partial p}{\partial \varphi} + \frac{\bar{w}}{c}u = 0 \tag{26}$$

Note that Equation (24) is nonlinear in u and we will restrict the solution to the region in which the grazing flow velocity dominates the orifice velocity. An approximate nonlinear solution can probably be found following the method of Reference 15 but that will not be attempted here. A discussion of the range of validity of the linear solution will be expanded upon in a later section. With this restriction in mind, Equation (24) can be written as

$$\left(\frac{\omega d}{c}\right)\frac{\partial u}{\partial t} + \frac{\bar{u}}{c}\frac{\partial u}{\partial r} + \left(\frac{\mathscr{P}}{\bar{\rho}cU_0}\right)\frac{\partial p}{\partial r} = 0 \tag{27}$$

The boundary conditions to be applied involve the excitation pressure imposed upon the system in the far field and the inevitable separation of the flow at the upstream edge of the orifice for inflow. This separation implies that for sufficiently short orifices (no reattachment) the ambient or back cavity pressure will be felt at the upstream orifice edge. This separation region is shown in Figure 2. For outflow the orifice boundary condition would be modified and it is thought that the solutions could be made to model outflow. This is not done in this paper and the solutions which follow are intended for inflow only at this time. The boundary conditions can be expressed as follows

$$p \to e^{it} \quad \text{as} \quad r \to \infty \tag{28}$$

$$p = 0 \quad \text{at} \quad r = r_0, \ \theta = \frac{\pi}{2}, \ \varphi = 0 \tag{29}$$

Solution to Differential Equations

The solution to the differential equations follow in a similar manner to that of Reference 15. Equation (23) can be immediately integrated to give,

$$u = -\frac{A}{r^2} F(t) \tag{30}$$

where the negative sign was chosen since the velocity is opposite to the radial coordinate for inflow. The function $F(t)$ depends upon t only since u was assumed not to be a function of θ or φ. Using Equation (30), Equation (27) can be written,

$$\frac{\partial}{\partial r}\left[\left(\frac{\omega d}{c}\right)\frac{A}{r}\frac{dF}{dt} - \frac{\bar{u}}{c}\frac{A}{r^2}F + \left(\frac{\mathscr{P}}{\bar{\rho}cU_0}\right)P\right] = 0 \tag{31}$$

Equation (31) can be integrated to obtain,

$$\left(\frac{\omega d}{c}\right)\frac{A}{r}\frac{dF}{dt} - \frac{\bar{u}}{c}\frac{A}{r^2}F + \left(\frac{\mathscr{P}}{\bar{\rho}cU_0}\right)p = f(t) \tag{32}$$

Use Equation (28) in Equation (32) as $r \to \infty$ to obtain,

$$f(t) = \left(\frac{\mathscr{P}}{\bar{\rho} c U_0}\right) e^{it} \tag{33}$$

where f(t) can be only a function of time due to the boundary condition of Equation (28). Thus, Equation (32) can be written,

$$\left(\frac{\omega d}{c}\right)\frac{A}{r}\frac{dF}{dt} - \frac{\bar{u}}{c}\frac{A}{r^2}F + \left(\frac{\mathscr{P}}{\bar{\rho} c U_0}\right)(p - e^{it}) = 0 \tag{34}$$

In solving for F(t) we will seek solutions of the form,

$$F(t) = e^{i(t+\delta)} \tag{35}$$

Substituting Equation (35) into Equation (34) and imposing the upstream boundary condition (Eq. (29)) at the orifice edge, after considerable arithmetic, A and δ can be determined such that

$$A = \frac{\mathscr{P} r_0}{\bar{\rho} U_0 \sqrt{(\omega d)^2 + \left(\frac{\bar{u}}{r_0}\right)^2}} \tag{36}$$

and

$$\tan \delta = -\frac{\omega d r_0}{V_\infty} \tag{37}$$

Using Equations (35), (36), and (37) in Equation (30) yields,

$$u = \frac{-\mathscr{P}(V_\infty - i\omega d r_0)}{\bar{\rho} U_0 \left[V_\infty^2 + (\omega d r_0)^2\right]} \left(\frac{r_0}{r}\right)^2 e^{it} \tag{38}$$

and then Equation (34) will give,

$$p = \frac{e^{it}\left\{\begin{array}{l}(\omega d r_0)^2\left(1-\frac{r_0}{r}\right)+V_\infty^2\left[1-\left(\frac{r_0}{r}\right)^2\sin\theta\cos\varphi\right] \\ -i\omega d r_0 V_\infty\left(\frac{r_0}{r}\right)\left[1-\left(\frac{r_0}{r}\right)\sin\theta\cos\varphi\right]\end{array}\right\}}{\left[V_\infty^2+(\omega d r_0)^2\right]} \tag{39}$$

It should be noted here that the velocity and pressure Equations (38) and (39) also satisfy the θ and φ momentum Equations (25) and (26).

ACOUSTIC IMPEDANCE

Before calculating acoustic impedance one more point must be made. Usually impedance is based upon the velocity calculated from orifice flow rates and orifice area. Note that the area of the hemisphere at $r = r_0$ is twice the orifice area. The value of u calculated at $r = r_0$ will thus be doubled when used to calculate impedance.

The acoustic impedance will be defined as the far field perturbation pressure divided by the orifice velocity and then normalized by $\bar{\rho}c$ or

$$\zeta = \frac{p'}{\bar{\rho}cu'_{orf}} = \frac{\mathscr{P}e^{it}}{\left(2\bar{\rho}cU_0 u\right)_{r_0}} \tag{40}$$

Using Equation (38) evaluated at $r = r_0 = 1/2$ in Equation (40) yields,

$$\zeta = -\frac{1}{2}\left(M_\infty + i\frac{\omega d}{2c}\right) \tag{41}$$

The negative sign occurs in Equation (41) because the velocity for inflow is in the negative r direction with the coordinate system centered on the orifice.

A dicsussion of Equation (41) along with a comparison with experimental data will be made in a later section.

Steady Orifice Inflow Theory

The theory of the preceding sections can be easily converted to a steady orifice inflow theory. This is useful since the theory can then be compared to the more easily obtained and thus more numerous steady flow data. This conversion to steady flow can most easily be obtained by letting $\omega \to 0$ (thus also eliminating $e^{it} = e^{i\omega t^*}$) in Equations (38) and (39). These equations thus become,

$$u_s = -\frac{\mathscr{P}}{\bar{\rho} U_0 V_\infty} \left(\frac{r_0}{r}\right)^2 \tag{42}$$

and

$$p_s = 1 - \left(\frac{r_0}{r}\right)^2 \sin\theta \cos\varphi \tag{43}$$

Some interesting results can be derived from the equations. First notice in Equation (43) that at the upstream edge of the orifice ($r = r_0$, $\theta = \pi/2$, $\varphi = 0$) that $p_s = 0$ which of course was the boundary condition reflecting flow separation at this point. The back cavity pressure is felt here. However at the downstream edge ($r = r_0$, $\theta = \pi/2$, $\varphi = \pi$), $p_s = 2$ or twice the far field pressure. In fact if the pressure is integrated over a hemisphere around the orifice to find an average pressure, it is found that this average is equal to the far field driving pressure. The pressure has just redistributed due to the grazing flow. The pressure in the high pressure region of the flow must yet be relieved in passing to the back cavity which requires a further expansion. In other words, the average pressure at $r = r_0$ still has a magnitude $\mathscr{P}$. The fluid must expand to have zero pressure as it passes to the back cavity side of the orifice. The velocity will thus increase

to a maximum at the vena-contracta. This will be analyzed using a one-dimensional approach to find an average vena-contracta velocity, u'_{vc}, and then a discharge coefficient will be calculated.

The further expansion in the orifice can be estimated from the Bernoulli equation,

$$\mathscr{P} = \frac{1}{2}\bar{\rho}\left[u'^2_{vc} - \left(U_0 u_s\right)^2\right] \tag{44}$$

where $U_0 u_s$ is the dimensional perturbation velocity at $r = r_0$, and the pressure drop is from $\mathscr{P}$ to zero in the back cavity. Using Equation (42) there results,

$$u'_{vc} = \sqrt{\frac{2\mathscr{P}}{\bar{\rho}} + \left(\frac{\mathscr{P}}{\bar{\rho}V_\infty}\right)^2} \tag{45}$$

From flow continuity considerations (use Eq. (42)) to calculate flow rate through the hemispherical area) the full flowing orifice velocity (based on orifice area and flow rate) is,

$$u'_{orf} = \frac{2\mathscr{P}}{\bar{\rho}V_\infty} \tag{46}$$

The orifice discharge coefficient is defined here as the ratio of the full flowing orifice velocity to the vena-contracta velocity and can then be calculated from

$$c_D = \frac{u'_{orf}}{u'_{vc}} = \frac{\sqrt{\dfrac{u'_{orf}}{V_\infty}}}{\sqrt{1 + \dfrac{\mathscr{P}}{2\bar{\rho}V^2_\infty}}} \approx \sqrt{\frac{u'_{orf}}{V_\infty}} \tag{47}$$

where $\mathscr{P}/2\bar{\rho}V^2$ was assumed to be small compared to unity.

This result has been found empirically in Reference 14 and will be discussed further in the next section along with pressure measurement comparisons using Equation (43).

DISCUSSION OF RESULTS

In this section the previously derived theory will be compared to data where it is available. The acoustic resistance is well established by experimental data. The acoustic inductance is less defined since measurements lump both the orifice end effects and within the orifice mass effects into one inductive quantity without any way of separating them. Also the steady orifice inflow theory will be compared to experiments.

Acoustic Impedance

Acoustic resistance. - The real part of Equation (41) (resistance) compares well with published experimental results. It is well established that resistance depends upon the grazing flow Mach number.

The coefficient of M_∞ in Equation (41) is 0.5 which compares favorably with 0.3 from References 4 and 7 for arrays of orifices and with 0.7 from Reference 14 for a single orifice. It is not intended that these theoretical results replace the empiricisms since there is much more work to be done on the details of the flow within the orifice, but only to show that the theory appears reasonable.

Acoustic reactance. - The theoretical results for orifice reactance are not so easily compared to data as was resistance. Since the major conclusions of this paper concern the reactance, it is best to first put the theory and the actual flow into proper perspective. Figure 2 shows sketches of the inflow to the orifice for conditions such that the grazing flow is completely dominant as assumed in the present theory. The flow patterns of figure 2 have been established for steady orifice flow in Reference 14 and for oscillatory orifice flow in Reference 16. The hemisphere of radius equal to the orifice radius is shown on Figure 2 and the solutions given in this paper are expected to apply outside of this hemisphere. The total inductance is determined by adding the inductance provided by the fluid within this hemisphere and within the orifice itself to the inductive orifice end correction given by Equation (41). Going back for a moment to zero grazing flow and low

pressure amplitudes, the orifice inductive end correction is given by 0.85d (Ref. 18) which would give 0.425d at each end of the orifice. Equation (41) accounts for over half (0.25d) of this correction which is outside of the hemisphere shown in Figure 2 with the remainder being within this hemisphere. Hard conclusions can thus be made about only half of this mass, but it is suspected that the conclusions will apply to the bulk of the attached mass.

Experimental data (Refs. 6, 8, and 17) show that the total inductance is reduced with a grazing flow. Since Equation (41) shows the inductive orifice end correction to be independent of grazing flow velocity, then the reduction in inductance which is observed must be coming from the fluid within or very close to the orifice. This conclusion is contrasted to the idea in which an orifice slug flow exists with an attached mass end correction which is blown away by the grazing flow.

Additional study must be devoted to the flow in the orifice. The orifice flow (with a grazing flow velocity) is not a slug which accommodates more mass flow by an acceleration of the slug. Instead the flow may have very nearly a constant velocity (see Ref. 16) with additional mass flow accommodated by an increased flow area. A sketch of these flow patterns is shown in Figure 3. It may be that a constant velocity, variable area type of flow has essentially no inductance at all. This latter point is currently being studied.

Steady Orifice Flow

For steady inflow into an orifice some discharge coefficient data are given in Reference 14. At low orifice velocity to grazing flow velocity ratios a fit to that data can be made as

$$c_D \approx 0.9 \sqrt{\frac{u'_{orf}}{V_\infty}} \tag{48}$$

This result compares favorably with the theoretical result of Equation (47).

In Reference 14 some pressure tap data was given in the vicinity of the orifice for both upstream and downstream locations. The data is given as $(p^* - p^*_\infty)/q_\infty$. For upstream pressure, Equation (43) gives

$$p_s = 1 - \left(\frac{r_0}{r}\right)^2 \tag{49}$$

where $\theta = \pi/2$, $\varphi = 0$ were used.

Equation (49) can be converted to (using Eq. (46)),

$$\frac{p_s^* - p_\infty^*}{\frac{1}{2}\bar{\rho}V_\infty^2} = -\frac{u'_{orf}}{V_\infty}\left(\frac{r_0}{r}\right)^2 \tag{50}$$

This is plotted in Figure 4 along with the results from Reference 14. The radius values used were $r/r_0 = 1.47$ which was determined by the dimensions shown on the figure insert. The agreement between the theory and the data are seen to be reasonably good.

For downstream pressure taps the analog of Equation (50) is,

$$\frac{p_s^* - p_\infty^*}{\frac{1}{2}\bar{\rho}V_\infty^2} = \frac{u'_{orf}}{V_\infty}\left(\frac{r_0}{r}\right)^2 \tag{51}$$

where $\theta = \pi/2$ and $\varphi = \pi$ was used in Equation (43). This result is also shown in Figure 4 along with data from Reference 14. The radius values here were $r/r_0 = 1.20$ determined from the dimensions from the insert on Figure 4. The odd behavior of the data at very low orifice flow was caused by the vortex standing in the orifice, which raised the streamlines above the orifice, and slightly depressed the downstream pressure. Once this depression effect is overcome by going to larger values of u'_{orf} the theory and the data agree quite well. In fact, the agreement for both curves in Figure 4 extends beyond the expected range of validity of the solution which will be discussed next.

RANGE OF VALIDITY OF THE LINEAR SOLUTION

Recall that the r-momentum Equation (24) was actually nonlinear and that this nonlinearity was ignored in the solutions of this paper. The coefficient of

the second term in Equation (24) may be written,

$$(\bar{u} + U_0 u) = - V_\infty \sin \theta \cos \varphi + U_0 u \tag{52}$$

In the area where the first term of the equation dominates the second term, the present solution might be expected to approximate the complete solution. This may be true provided the area of influence of the nonlinearity is small. The coordinates of the flow area at which the two influences are equal is given by,

$$\sin \theta \cos \varphi = \frac{U_0 u}{V_\infty} \tag{53}$$

The nonlinear solution is approximated from the results of Reference 15 (and ignoring the time dependence) as

$$U_0 u \approx \sqrt{\frac{\mathscr{P}}{\bar{\rho}}} \tag{54}$$

thus Equation (53) becomes

$$\sin \theta \cos \varphi \approx \sqrt{\frac{\mathscr{P}}{\bar{\rho} V_\infty^2}} \tag{55}$$

The ratio of the flow area dominated by the nonlinear solution to that of the entire area may be estimated by (assuming $\mathscr{P}/\bar{\rho}V_\infty^2$ is very small),

$$\frac{A_{NL}}{A_{TOT}} \approx \frac{4}{\pi} \sqrt{\frac{\mathscr{P}}{\bar{\rho} V_\infty^2}} \tag{56}$$

Mass flow rates in the two regions (rather than areas) could also have been used to indicate the importance of the nonlinearity. Using Equation (46), Equation (56) becomes,

$$\frac{A_{NL}}{A_{TOT}} \approx \frac{2\sqrt{2}}{\pi} \sqrt{\frac{u'_{orf}}{V_\infty}} \tag{57}$$

Thus it is presumed that as long as the quantity on the right side of Equation (57) is small, then the nonlinearity can be ignored. Note from Equation (52) (when $\sin\theta \cos\varphi \approx 0$) that the nonlinear term should dominate when $\theta = 0$ or $\varphi = \pi/2$ or $3\pi/2$ which is above and to the sides of the orifice (in the y-z plane of Fig. 1). Also note from Equation (43) (again $\sin\theta \cos\varphi \approx 0$) that this is precisely the region in which the linear solution would predict that the pressure is equal to the far-field driving pressure (both equal to one). Thus with an apparent lack of driving pressure difference in the nonlinearly dominated area, the linear solution may be valid well beyond the criterion given above (the right side of Eq. (57) being small). This may explain the agreement between the linear theory and the data shown in Figure 7 well beyond the u'_{orf}/V_∞ range at first expected. Thus it is anticipated that for the usual acoustic pressures and grazing flow velocities found in aircraft suppressors, the nonlinearity and thus the nonlinear acoustic resistance due to the acoustic pressure will be negligible.

CONCLUDING REMARKS

The main conclusion of this paper is that the orifice inductive and correction or attached mass is not a function of grazing flow velocity. This was shown by calculating the acoustic impedance in Equation (41) and observing the inductance term. This conclusion could also be drawn from the governing differential Equation (27). Only the first term in this differential equation can contribute to velocity components which are out of phase with the pressure and this term does not contain the grazing flow velocity. This approach (using the differential equation) is more general since now also the orifice outflow can be included if it is assumed the small separated flow leaving the orifice near the wall on the downstream side does not appreciably affect the reactive part of the solution.

When the nonlinearity (small for u'_{orf}/V_∞ mush less than unity) is restored to the differential Equation (24) then the conclusions must be modified somewhat. The nonlinearity can produce reactive changes as shown in Reference 15 but these effects, especially their dependence upon grazing flow, will be unknown

until the nonlinear solution is obtained. However, it has been argued here that this nonlinearity is probably not important except at extremely high pressure amplitudes and small grazing flows for which u'_{orf}/V_∞ would become large.

If the inductance change with grazing flow does not come from the attached mass (orifice inductive end effect) then it must be coming from the flow within the orifice itself. This region is a prime candidate for this effect since the flow within the orifice may have close to a uniform velocity with mass flow changes occurring due to a variable flow area.

The acoustic resistance was calculated using the theoretical results presented here. The resistance was shown to depend linearly upon the grazing flow velocity with a magnitude agreeing quite well with published data. Since the nonlinearity in the differential equation does not seem to play an important role, this implies that the resistance will be dominated by the grazing flow and will not be sensitive to the acoustic pressure.

It should be recalled that the solutions to the differential equations provided here are for the flow perturbations. To obtain the complete pressure and velocity solutions, these perturbations must be added to the average pressure and uniform grazing flow velocities.

The complete solution to the orifice impedance problem is yet to be obtained. This will involve the coupling of the solutions on the cavity side of the orifice, the complicated three-dimensional orifice flow, and the grazing flow side of the orifice for both inflow and outflow.

REFERENCES

1. B. Phillips, "Effects of High Wave Amplitude and Mean Flow on a Helmholtz Resonator," NASA TM X-1582 (May 1968).

2. "Suppression of Combustion Oscillations with Mechanical Damping Devices," Pratt and Whitney Aircraft Rept. FR-4993 (June 1971); also NASA CR-123721.

3. G. D. Garrison, et al.: "Suppression of Combustion Oscillations with Mechanical Devices," Pratt and Whitney Aircraft Rept. TR-3299 (Aug. 1969); also NASA CR-107102.

4. E. Elder, and L. W. Dean, "Analytical and Experimental Studies for Predicting Noise Attenuation in Acoustically Treated Ducts for Turbofan Engines," NASA CR-1373 (Sept. 1969).

5. M. Budoff and W. E. Zorumski, "Flow Resistance of Perforated Plates in Tangential Flow," NASA TM X-2361 (Oct. 1971).

6. D. L. Armstrong, "Acoustic Grazing Flow Impedance Using Waveguide Principles," Boeing Co. Rept. D3-8684 (Dec. 1971); also NASA CR-120848.

7. E. J. Rice: A Model for the Acoustic Impedance of a Perforated Plate Liner with Multiple Frequency Excitation. NASA TM X-67950 (1971).

8. D. Ronneberger, "The Acoustic Impedance of Holes in the Wall of Flow Ducts," J. Sound Vib., 24, 133 (1972).

9. P. D. Dean, "An In Situ Method of Wall Acoustic Impedance Measurement in Flow Ducts," J. Sound Vib., 34, 97 (1974).

10. E. Feder, "Effect of Grazing Flow Velocity on the Steady Flow Resistance of Duct Liners," Pratt and Whitney Aircraft Rept. 5051 (1974).

11. P. D. Dean and B. J. Tester: Duct Wall Impedance Control as an Advanced Concept for Acoustic Suppression. NASA CR-134998 (1976).

12. W. A. Sirignano and T. S. Tonon, "Nonlinear Aspects of Combustion Instability in Liquid Rocket Motors," Princeton Univ. Rept. AMS-SR-553-h (June 1968); also NASA CR-72426.

13. B. T. Zinn, "A Theoretical Study of Nonlinear Damping by Helmholtz Resonators," AIAA Paper 69-481, Colorado Springs, Colo. (June 1969).

14. T. Rogers and A. S. Hersh, "The Effect of Grazing Flow on the Steady-State Resistance of Isolated Square-Edged Orifices," AIAA Paper 75-493, Hampton, Va. (Mar. 1975). Also NASA CR-2681.

15. A. S. Hersh and T. Rogers: Fluid Mechanical Model of the Acoustic Impedance of Small Orifices. AIAA Paper 75-495, Hampton, Va. (Mar. 1975). Also NASA CR-2682.

16. K. J. Baumeister and E. J. Rice, "Visual Study of the Effect of Grazing Flow on the Oscillatory Flow in a Resonator Orifice," NASA TM X-3288 (Sept. 1975).

17. F. Mechel, P. Mertens, and W. Shilz, "Research on Sound Propagation in Sound Absorbent Ducts with Superimposed Air Streams," Gottingen u. Physikalisches Inst. (West Germany) (Dec. 1962); ARML-TDR-62-140(III).

18. U. Ingard and H. Ising, "Acoustic Nonlinearity of an Orifice," J. Acoustic Soc. Am., 42 (1967).

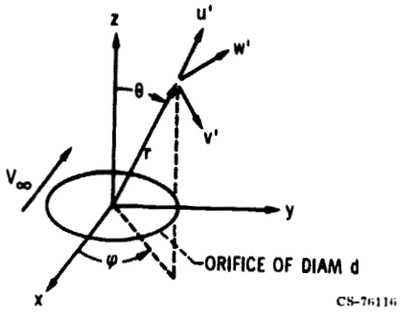

Figure 1. - Geometry used in orifice flow analysis.

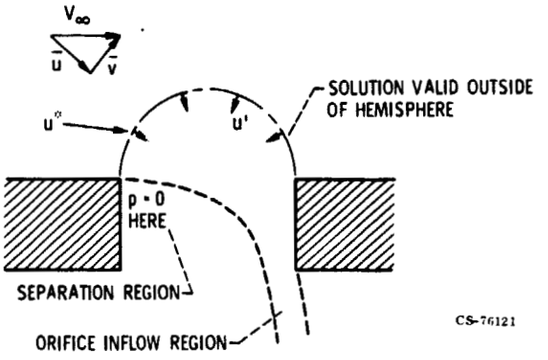

Figure 2. - Sketch of orifice inflow with a grazing flow.

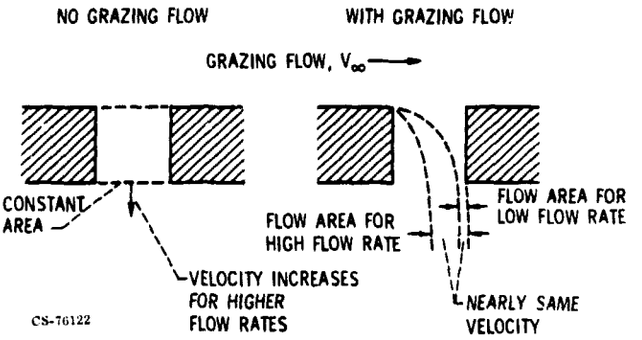

Figure 3. - Sketch of orifice flow patterns.

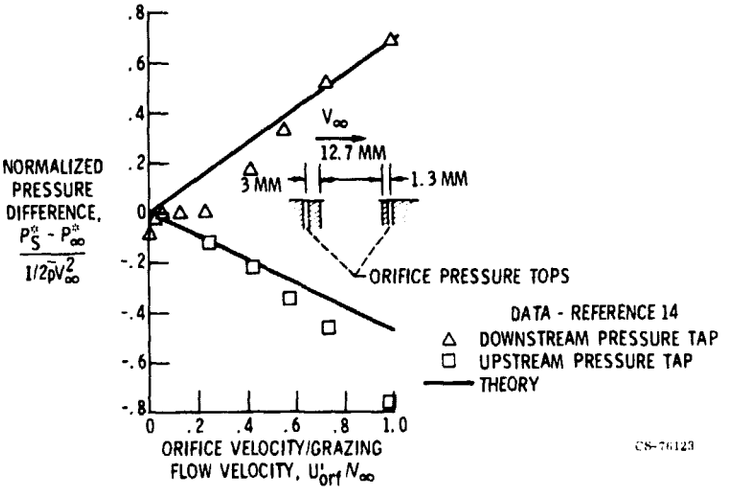

Figure 4. - Comparison of measured and theoretical static pressures near an orifice.